Applied Surface Science 257 (2011) 2779–2790

Applied Surface Science

journal homepage: www.elsevier.com/locate/apsusc

Influence of physicochemical–electronic properties of transition metal ion doped polycrystalline titania on the photocatalytic degradation of Indigo Carmine and 4-nitrophenol under UV/solar light

L. Gomathi Devi*, S. Girish Kumar

Department of Post Graduate Studies in Chemistry, Central College City Campus, Dr. Ambedkar street, Bangalore University, Bangalore 560001, India

ARTICLE INFO

Article history:
Received 5 May 2010
Received in revised form 1 September 2010
Accepted 14 October 2010
Available online 21 October 2010

Keywords:
Transition metal ion doped titania
Electronic configuration of dopant
Physicochemical–electronic properties of doped titania
Synergistic effect
Vectorial interparticle electron transfer

ABSTRACT

To understand the role of dopant inside TiO_2 matrix, anatase TiO_2 was doped with transition metal ions like Mn^{2+}, Fe^{3+}, Ru^{3+} and Os^{3+} having unique half filled electronic configuration and their photocatalytic activity was probed in the degradation of Indigo Carmine (IC) and 4-nitrophenol (NP) under UV/solar light. For comparison, TiO_2 was also doped with V^{5+}, Ni^{2+} and Zn^{2+} metal ions having d^0, d^8 and d^{10} electronic configuration respectively. Irrespective of excitation source UV/solar light and nature of the organic pollutant, photocatalytic activities of doped photocatalysts followed the order: Mn^{2+}-TiO_2 > Fe^{3+}-TiO_2 > Ru^{3+}-TiO_2 ≥ Os^{3+}-TiO_2 > Zn^{2+}-TiO_2 > V^{5+}-TiO_2 > Ni^{2+}-TiO_2 at an optimum concentration of dopant. Based on the experimental results obtained, it is proposed that the existence of dopant with half filled electronic configuration in TiO_2 matrix which is known to enhance the photocatalytic activity is not universal! Rather it is a complex function of several physicochemical–electronic properties of doped titania. Enhanced photocatalytic activity of Mn^{2+} (0.06 at.%)-TiO_2 was attributed to the combined factors of high positive reduction potential of Mn^{2+}/Mn^{3+} pairs, synergistic effects in the mixed polymorphs of anatase and rutile, smaller crystallite size with high intimate contact between two phases and favorable surface structure of the photocatalyst. Despite the intense research devoted to transition metal ion doped TiO_2, it is rather difficult to make unifying conclusion which is highlighted in this study.

1. Introduction

Heterogeneous photocatalysis using semiconductor metal oxide materials has attracted enormous amount of research interest since the first electrochemical cell for water splitting was reported by Fujishima and Honda [1]. Semiconductors like $Bi_{12}TiO_{20}$ [2], Nb_2O_5 [3], $Sm_2Ti_2S_2O_5$ [4], Bi_2O_3 [5], $ZnWO_4$ [6], Bi_2WO_6 [7], $NaTaO_3$ [8], $CaIn_2O_4$ [9], WO_3 [10], TiO_2 [11], Fe_2O_3 [12], ZnO [13], etc, finds extensive application either in water splitting/degradation of organic compounds. Among the various semiconductors, TiO_2 is extensively used photocatalyst due to its chemical and biological inertness, water insolubility, non-toxicity, resistance against photo-chemical corrosion and its cheap availability. TiO_2 is very important multifunctional material because of its peculiar and fascinating physicochemical–optical properties and wide variety of potential uses in diverse fields such as solar energy conversion, conventional purification and wastewater treatment. The band gap excitation of TiO_2 by suitable light energy generates charge carrier pairs with robust redox properties that may recombine, become trapped in metastable surface state or react with electron acceptors/donors adsorbed on the surface of the photocatalyst. However, the high degree of recombination between photogenerated charge carriers in TiO_2 and also its large band gap limits its overall photocatalytic efficiency. An intense research has been devoted in recent years to lower the threshold excitation energy in order to utilize large fraction of solar light with high efficiency by several methods which mainly includes metal ion doping [14–25], non metal ion doping [26–35], surface sensitization of TiO_2 by dyes [36–38] and metal complexes [39,40], coupling with narrow band gap semiconductor [41,42] and depositing noble metal on the TiO_2 surface [43,44].

The transition metal ion doping in the titania matrix, changes the local electronic structure and induces the visible light absorption usually by introducing localized electronic states within the band gap and it also creates different surface structure that can intrinsically alter the surface transfer of charge carriers and hence the photocatalytic activity [14–25]. Despite the intensified research on metal ion doped TiO_2, no unifying decision has been made so far, since wide variety of experimental conditions applied for photocatalyst preparation and different substrates chosen to study their activity. For instance, Nagaveni et al. reported the doping of metal

* Corresponding author. Tel.: +91 80 22961336; fax: +91 80 22961331.
E-mail address: gomatidevi_naik@yahoo.co.in (L.G. Devi).

0169-4332/$ – see front matter © 2010 Elsevier B.V. All rights reserved.
doi:10.1016/j.apsusc.2010.10.062

ions like W, Fe, Ce, V, Cu and Zr into TiO_2 lattice was not beneficial for the degradation of 4-chlorophenol [45], while some groups claims the enhanced activity for the same dopants under different experimental reaction conditions. Herrmann et al. reported that the recombination rate of electron–hole pair increases for chromium doped TiO_2 [46], while Wilke and Breuer suggested the correlation between the lifetime of charge carriers and the photocatalytic activity for TiO_2 doped with Cr^{3+} and Mo^{5+} ions [47]. TiO_2 doped with Mo and V ions exhibited significantly reduced photoactivity [48], although Gratzel and Howe suggested an inhibition of electron–pair recombination with these dopants based on EPR data [49]. Mu et al. reported that doping TiO_2 with trivalent or pentavalent metal ions was detrimental to the photocatalytic reactivity [50], while Karakitsou and Verykios showed that doping with hypervalent cations enhanced the activity [51]. A comparison among the results reported in the literature for the photocatalytic activity of doped titanates obtained from various preparations is not very easy because the experimental conditions under which the runs are carried out and the preparation methods of the photocatalysts are usually different. As a matter of fact, the different synthetic procedures used each time to synthesize metal ion doped titania and the different types of pollutants used for photodegradation studies create a varying set of data that can frequently become controversial!

Choi et al. systematically studied the effect of doping different metal ions into Q-TiO_2 matrix for chloroform oxidation and carbon tetrachloride reduction. The higher activity for Fe^{3+} doped titania compared to other metal ion doped samples was attributed to unique stable half filled electronic structure of Fe^{3+} ion which was predicted to serve as shallow traps for the charge carriers [15]. Xu et al. also reported the enhanced activity of Gd^{3+} doped TiO_2 for the decomposition of nitrate compared to other rare earth doped samples due to the stable half filled electronic configuration of Gd^{3+} ion [52]. Similar reports are also available in the literature claiming the enhanced activity of the doped titania with dopant having half filled electronic configuration compared to other dopants possessing different electronic configuration [53,54]. Hence to probe the enhanced activity of metal ion doped TiO_2 with dopant being in half filled electronic structure is either universal or not? herewith we investigate the photocatalytic activities of TiO_2 doped with metal ions Mn^{2+}, Fe^{3+}, Ru^{3+}, and Os^{3+} ions having stable half filled electronic configuration. For comparison, other dopants like V^{5+}, Ni^{2+} and Zn^{2+} having vacant, partially and completely filled electronic configuration is also chosen to correlate the different electronic structure of various dopants influencing the photocatalytic activity of doped samples. The research work presents data, which are analyzed in the spirit of the above introduction and focuses in the rationalization of various physicochemical–electronic properties affecting the photocatalytic activity of transition metal ion doped titanates. The degradation of indigo carmine (IC) and 4-nitrophenol (NP) was chosen as model reaction under UV/solar light to evaluate the photocatalytic efficiency of the prepared photocatalysts.

2. Experimental

2.1. Preparation of photocatalysts

Polycrystalline anatase TiO_2 was synthesized by sol–gel route through the hydrolysis of titanium tetrachloride [55]. 25 ml of diluted $TiCl_4$ with 1 ml concentrated H_2SO_4 is taken in a beaker and diluted to 1000 ml. The pH of the solution was maintained at 7–8 by adding liquor ammonia. The gel obtained was allowed to settle down. The precipitate is washed free of chloride and ammonium ions. The gelatinous precipitate is filtered and oven dried at 100 °C. The finely ground powder was then calcined at 550 °C for 4.5 h. For the preparation of metal ion doped TiO_2 (M^{n+}-TiO_2), a known concentration of the metal ion solution was added to calculated amount of TiO_2 to get the dopant concentration in the range of 0.02–0.1 at.%. The obtained powder is ground in a mortar and oven dried at 120 °C for 1 h. The process is repeated for 3–4 times and the powder is finally calcined at 550 °C for 4.5 h [56–57].

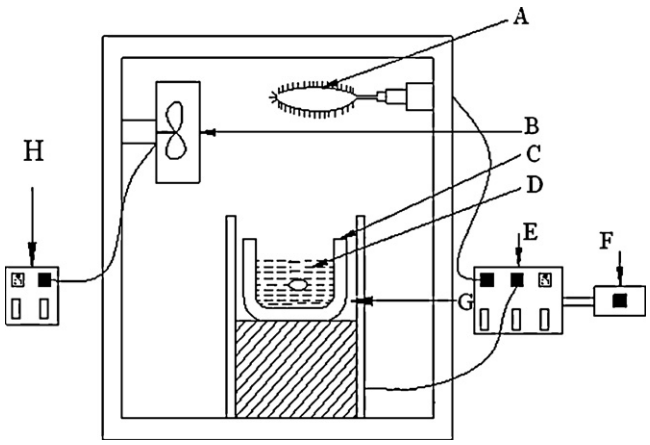

Fig. 1. Schematic diagram of reactor configuration. (A) Mercury vapor lamp, (B) fan, (C) glass reactor, (D) experimental solution, (E) stabilizer, (F and H) switch box, (G) thermostat.

2.2. Characterization

The crystallite phase of the sample and variation of lattice parameter upon doping with metal ions weredetermined by PXRD measurements using Philips powder diffractometer PW/1050/70/76 with Cu Kα radiation. The average crystallite size (D) was calculated using Scherer's eq.: $D = k\lambda/\beta \cos\theta$, where k is the shape factor (~0.9), λ is the X-ray wavelength (0.15418 nm), β is the full width at half maximum (FWHM) of the diffraction line and θ is the diffraction angle. The specific surface area of the powders were measured by dynamic Brunner–Emmet–Teller (BET) method in which N_2 gas was adsorbed at 77 K using Digisorb 2006 surface area, pore volume analyzer Nova Quanta Chrome corporation instrument multipoint BET adsorption system. The diffuse reflectance spectra (DRS) of the photocatalyst sample in the wavelength range of 200–700 nm were obtained by a UV–vis scanning spectrophotometer (31031 PC UV–vis–NIR instrument) using $BaSO_4$ as reference standard. The band gaps of photocatalysts were calculated by using Kubelka–Munk plot. The decrease in the concentration of IC/NP was quantified by UV–vis spectrophotometer using Shimadzu UV-1700 Pharmaspec UV–vis spectrophotometer.

2.3. Estimation of photocatalytic activity

The reactor configuration used for the degradation of organic pollutant is shown in Fig. 1. The photocatalytic degradation of IC/NP was performed with 300 mg of the photocatalyst suspended in optimized concentration of substrate in 250 mL aqueous solution under UV/solar light irradiation. Prior to photocatalytic reactions, the suspension was magnetically stirred in dark for 30 min to ensure adsorption equilibrium of substrate on the photocatalyst surface. Sample aliquots were withdrawn from the reactor at a specific time interval during the illumination and filtered to remove the photocatalyst particles. Duplicate or triplicate photocatalytic degradation experiments were carried out under each experimental condition to confirm the reproducibility. Artificial light source employed in the study is 125 W medium pressure mercury vapor lamp whose emission wavelength falls in the region 350–400 nm, with maximum emission at 370 nm. Natural solar light in the summer season

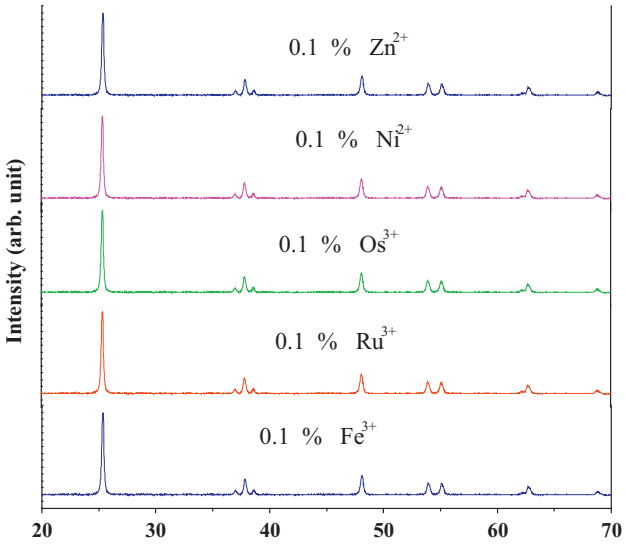

Fig. 2. PXRD patterns of various metal ion doped TiO_2 samples.

was used in the study to investigate visible light activity of photocatalysts. Experiments under solar light were carried out between 12 noon and 2 pm at which fluctuation in the solar intensity was minimal. The latitudes and longitudes are 12.58 N and 77.38 E respectively. The average intensity of the sunlight is found to be around 1200 W m^{-2} using radiometer [56–57]. All the experiments were performed using double distilled water in the presence of atmospheric oxygen.

3. Results and discussion

3.1. PXRD studies

The reflections for all the doped samples were indexed to anatase phase (Fig. 2), excluding Mn^{2+}-TiO_2 which showed mixed phases of anatase and rutile (Fig. 3). The rutile fraction in the sample was calculated using the Spurr and Meyer's Eqs. (1a) and (1b) [58]

$$X_R = \frac{1}{1 + 0.8\left(I_A/I_R\right)} \quad (1a)$$

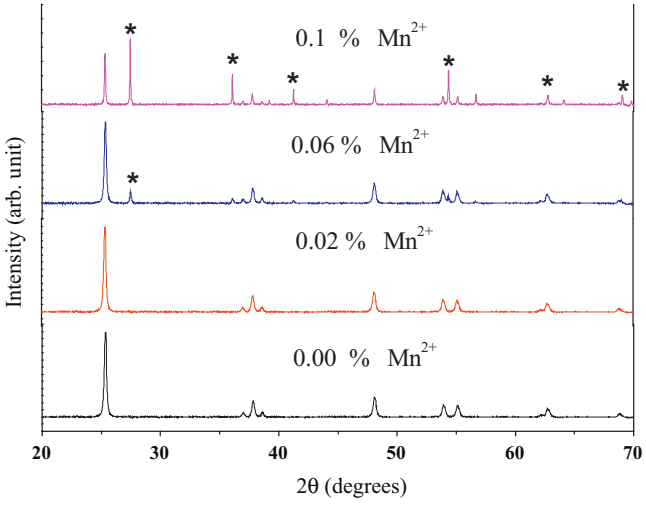

Fig. 3. PXRD patterns of Mn^{2+}-TiO_2 samples at different concentrations of Mn^{2+} ion. The peak with asterisk '*' corresponds to rutile phase.

$$X_R = 1 - X_A \quad (1b)$$

where X_A and X_R is the mass fraction of anatase and rutile respectively, I_A and I_R were the X-ray integrated intensities corresponding to the (1 0 1) diffraction plane of anatase and (1 1 0) of rutile phase, respectively.

The influence of dopant on the phase transformation can be well explained considering the nature of defects i.e., interstitial titanium and oxygen vacancies created in TiO_2. With respect to cationic impurities, the substitution of lower valent dopant ion compared to the host Ti^{4+} accelerates the phase transformation from anatase to rutile due to the formation of oxygen vacancies that enhances the transport of atoms within the anatase structure. On the other hand, the incorporation of higher valent dopant ion reatards the phase transformation for the formation of Ti^{3+} ion that suppress the atomic transport in the anatase structure [59].

The ionic radii of the dopants Fe^{3+} (0.64 Å), Ru^{3+} (0.69 Å), Os^{3+} (0.73 Å), V^{5+} (0.59 Å), Ni^{2+} (0.72 Å), Zn^{2+} (0.74 Å) were almost similar to that of host Ti^{4+} (0.68 Å) ions. From the view point of radius matching, it is possible for these metal ion dopants to substitute Ti^{4+} ion in TiO_2 lattice easily without distorting the crystal structure of pristine TiO_2 over a range of dopant concentration [15]. The higher ionic size of Mn^{2+} (0.80 Å) produces a localized charge distortion inducing oxygen vacancies which favors bond rupture, solid state ionic rearrangement and structure reorganization for rutile nucleation [60]. It is generally believed that oxygen vacancies induced in the anatase TiO_2 lattice promote the transport of atoms within the anatase structure resulting in rutile nucleation. At a dopant concentration of 0.06 at.%, the photocatalyst exhibited higher anatase:rutile ratio of 90:10, while at higher dopant concentration of 0.1 at.%, the sample showed higher rutile:anatase ratio of 52:48 (Table 1). The increase in the rutile fraction for Mn^{2+}-TiO_2 samples with simultaneous decrease in crystallite size provides a consistent evidence for the existence of crystallite size effect on anatase–rutile phase transformation. The smaller crystallite size will be associated with imperfect lattice defects at the surface. This imperfect surface may enhance the atomic diffusion and the small particle size may shorten the necessary atomic diffusion length for the phase transition. The higher rutile content for Mn^{2+} (0.1 at.%)-TiO_2, is mainly due to its smaller crystallite size which is believed to contain the high density of surface defects on the anatase crystallite. Thus the high concentration of nucleation sites for the polymorphic phase transition from anatase to rutile exists at particle-particle interfaces in comparison to bulk materials. Furthermore, the atoms in the defect sites have higher energy than those in the main lattice and can favorably act as nucleation sites for the rutile phase formation at the surface of anatase crystallites. The anatase to rutile phase transformation is generally considered as a nucleation growth during which the rutile nuclei are formed within the anatase phase. The anatase–rutile transformation is believed to be spontaneous because the free energy of rutile is always lower than that of anatase, but it is kinetically unfavorable at low temperature. Thus it can be concluded that activation energy barrier for phase transformation is significantly reduced due to the inclusion of Mn^{2+} in TiO_2 matrix which is in accordance with previous literature [61].

The variation in the lattice parameters were reflected in the elongation of '*c*' axis, with *a* (=*b*) remaining almost constant for all the doped samples [57]. Since only '*c*' dimension is changing while '*a* (=*b*)' remains almost constant for the range of dopant concentration, it can be concluded that dopant M^{n+} (M^{n+} = Mn^{2+}, Fe^{3+}, Ru^{3+}, Os^{3+}, V^{5+}, Ni^{2+}, Zn^{2+}) substitutes Ti^{4+} lattice sites preferentially on the bcc and fcc in the anatase structure [62]. Mn^{2+}-TiO_2 samples shows slight thermal expansion in the lattice structure due to the higher ionic size of Mn^{2+} compared to the host Ti^{4+} ion. Hence substitution of Mn^{2+} at Ti^{4+} lattice sites might induce some structural defects, such as oxygen vacancies mainly on the surface

Table 1
A:R phase composition, crystallite size (nm), specific surface area (m^2/g), band gap absorption (nm) and percentage degradation (% *D*) of IC under UV/solar light using various photocatalyts.

Photocatalyst[a]	*A:R*	Crystallite size	Surface area	Band gap absorption	% *D*	
					UV	Solar
TiO_2	100:0	26.2	18	380	38	07
V^{5+} (0.02%)-TiO_2	100:0	26.2	23	424	22	22
V^{5+} (0.06%)-TiO_2	100:0	26.3	26	456	35	31
V^{5+} (0.10%)-TiO_2	100:0	28.4	24	446	30	28
Mn^{2+} (0.02%)-TiO_2	100:0	23.6	21	426	68	56
Mn^{2+} (0.06%)-TiO_2	90:10	20.3:20.3	26	454	100	91
Mn^{2+} (0.10%)-TiO_2	48:52	16.6:16.6	24	420	25	38
Fe^{3+} (0.02%)-TiO_2	100:0	24.2	25	435	58	47
Fe^{3+} (0.06%)-TiO_2	100:0	21.6	33	474	74	64
Fe^{3+} (0.10%)-TiO_2	100:0	19.5	38	460	45	50
Ru^{3+} (0.02%)-TiO_2	100:0	23.8	23	445	48	41
Ru^{3+} (0.06%)-TiO_2	100:0	20.8	28	485	61	52
Ru^{3+} (0.10%)-TiO_2	100:0	19.1	36	471	45	38
Os^{3+} (0.02%)-TiO_2	100:0	23.1	24	436	54	41
Os^{3+} (0.06%)-TiO_2	100:0	20.1	30	492	55	49
Os^{3+} (0.10%)-TiO_2	100:0	19.5	35	476	50	45
Ni^{2+} (0.02%)-TiO_2	100:0	23.8	25	426	14	20
Ni^{2+} (0.08%)-TiO_2	100:0	18.9	40	468	24	22
Ni^{2+} (0.10%)-TiO_2	100:0	15.1	36	457	19	23
Zn^{2+} (0.02%)-TiO_2	100:0	23.6	24	420	35	23
Zn^{2+} (0.06%)-TiO_2	100:0	19.8	30	456	45	38
Zn^{2+} (0.10%)-TiO_2	100:0	15.6	31	442	40	30

[a] The dopant concentration is in atom% in Tables 1–3.

to partially compensate the lattice strain [63a]. Thus the imperfect surface in Mn^{2+}-TiO_2 may enhance atomic diffusion and favors rutile nucleation. The surface areas of all the doped samples were higher than undoped titania due to the introduction of additional nucleation sites by the dopants and also due to its smaller crystallite size (Table 1). Thus the change in the surface area, crystallite size and variation in the lattice parameters observed for all the doped samples confirms the possible substitution of dopants in Ti^{4+} lattice sites [56,57,61].

To confirm, whether dopant having higher ionic size than that of host Ti^{4+} ion, would induce phase transformation from anatase to rutile, Pd^{2+} were substituted for Ti^{4+} in TiO_2 in the range of 0.02–0.5% using $PdCl_2$ as a source for doping Pd^{2+}. In contrast to Mn^{2+}-TiO_2, we obtained mixed phase of anatase and rutile for Pd^{2+}-TiO_2 at a concentration of 0.5% (Fig. 4). The rutile fraction disappeared and PdO phase nucleated at higher dopant concentration. These results suggested that dispersed PdO particles on the anatase phase (which could not be detected by XRD) inhibited the rutile phase formation at higher dopant concentration. The significant growth of PdO phase diminished rutile phase in the samples, which reflects that dopant solubility in the TiO_2 matrix critically influences the phase transformation. Similar reports were also made by Chen et al. [63b], regarding the phase transformation of sol–gel TiO_2 doped with K^+ ions. Phase transformation from anatase to rutile was achieved at 1123 and 1273 K for bare TiO_2 and K^+ (4.6 mol%) doped TiO_2 sample. However, for a higher K^+ concentration, anatase and rutile phase became insignificant due to the formation of $K_{4-4x}Ti_xO_2$ complexes.

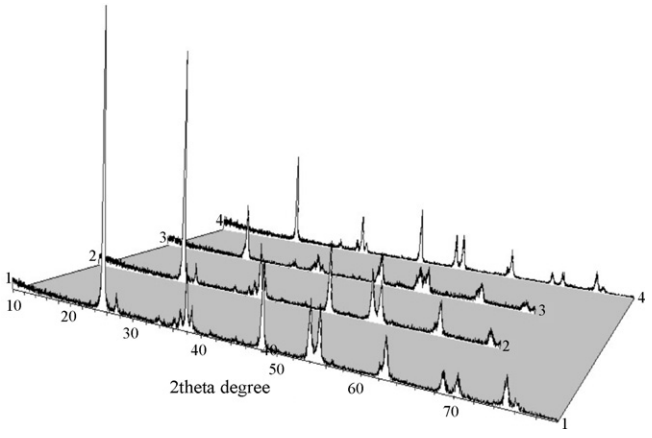

Fig. 4. PXRD patterns of Pd^{2+}-TiO_2 samples at various Pd^{2+} ion concentrations; (1) 0.5%; (2) 1.0%; (3) 2.0%; (4) 1.5% of Pd^{2+}.

3.2. DRS studies

The change in the electronic properties of TiO_2 upon doping with different metal ions was investigated using DRS technique. TiO_2 has strong absorption edge tailing at ~380 nm attributed to the band to band transition from O 2p level to Ti 3d level. The origin of visible spectra in the case of M^{n+}-TiO_2 is due to the formation of localized electronic states of the dopant within the band gap states of pristine TiO_2. The introduction of such electronic energy levels within the band gap states induces the red shift in the band gap transition and the visible light absorption through a charge transfer between energy level of dopant and band gap states of TiO_2 or by d–d transition in the crystal field. The DRS spectra reveals that undoped TiO_2 has no significant absorption band edge in the visible region, while all the doped samples exhibited marked increase in the band gap absorption at a dopant concentration of 0.06 at.%, excluding Ni^{2+} which showed large red shift in the band gap absorption at 0.08 at.% (Table 1 and Fig. 5). The sequence of reducing the band gap excitation energy in the doped samples among the various dopants followed the order: $Os^{3+} \sim Ru^{3+} > Fe^{3+} \sim Ni^{2+} > Zn^{2+} \sim Mn^{2+} \sim V^{5+}$ (Table 1). Although the position of localized electronic interband of dopant depends on their d electron configuration and distribution of metal ions in the TiO_2 matrix, the sequence obtained also shows that the band gap absorption can also depend on the electronegativity of the substituted dopant. Plot of band gap energy of the prepared samples as a function of inverse electronegativity of the dopant display roughly/almost linear relationship, although the types of d orbital contribution are different by the dopants (Mn^{2+}, V^{5+}, Ni^{2+}, Zn^{2+}, Fe^{3+} contributes 3d electronic level, while Ru^{3+} and Os^{3+} contributes

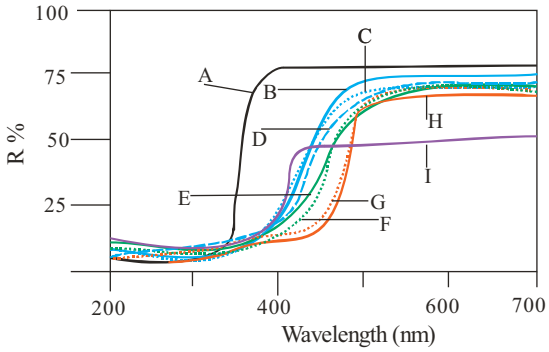

Fig. 5. UV–vis diffuse reflectance spectra of various photocatalysts. (A) TiO_2; (B) Mn^{2+} (0.06%)-TiO_2; (C) V^{5+} (0.06%)-TiO_2; (D) Zn^{2+} (0.06%)-TiO_2; (E) Fe^{3+} (0.06%)-TiO_2; (F) Ni^{2+} (0.08%)-TiO_2; (G) Ru^{3+} (0.06%)-TiO_2; (H) Os^{3+} (0.06%)-TiO_2; (I) V^{5+} (0.02%)-TiO_2.

4d and 5d electronic level, respectively). This finding illustrates that the inverse electronegativity of the substituted dopant can be a semiquantitative measure for tailoring the band gap energy of TiO_2 in the present study (Fig. 6). Hur et al. reported the visible light photocatalytic activity of strontium indium niobate doped with Pb^{4+} and Sn^{4+} for the degradation of 4-chlorophenol. Since the substituted Pb^{4+} and Sn^{4+} are more electronegative than In^{3+}, the Pb 6s and Sn 5s electronic states were expected to have lower energy than In 5s electronic state. The large shift in the band gap absorption in Pb^{4+} doped samples compared to Sn^{4+}, was attributed to higher electronegativity of Pb^{4+} in comparison with Sn^{4+} [64a]. The similar red shift in the band gap absorption values of Zn^{2+}-TiO_2 and V^{5+}-TiO_2 was mainly attributed to the similarity in the electronegativity of both the dopants [57a]. Further, large shift in the band gap absorption for Mo^{6+}-TiO_2 in comparison with Mn^{2+}-TiO_2 was accounted to the higher electronegativity of Mo [53]. The results obtained in the present study are in good agreement with the studies of Hur et.al [64a]. The tailing of absorption band in the visible region can also be attributed to the charge transfer transition between the interacting ions [17a]:

$$M^{n+} + M^{n+} \rightarrow M^{(n+1)+} + M^{(n-1)+} \quad (2)$$

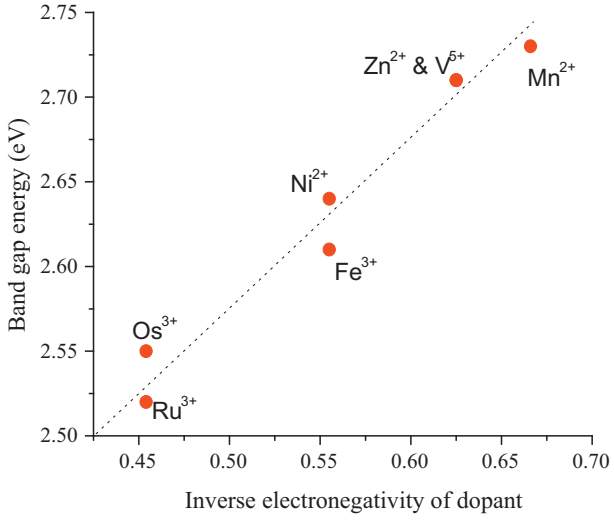

Fig. 6. Plot of inverse electronegativity of dopant as a function of band gap absorption in the respective doped catalysts at opitimum dopant concentration.

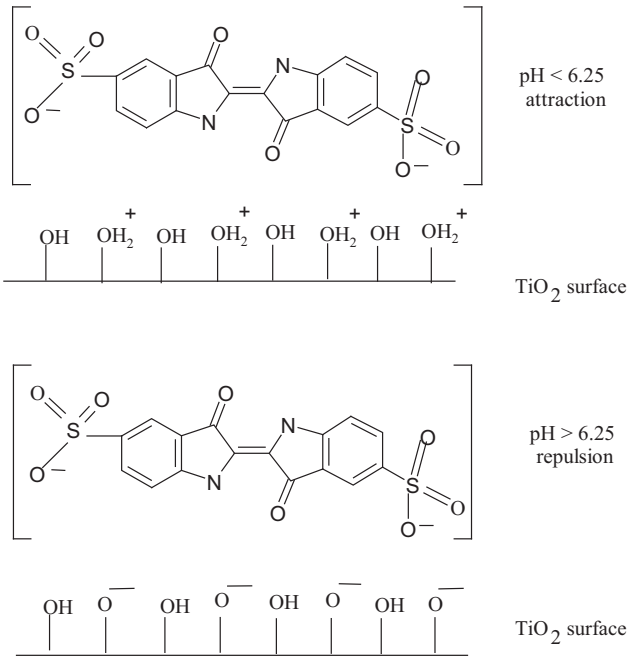

Fig. 7. Surface charges above and below the iso electric point of TiO_2 showing the electrostatic attraction and repulsion of the IC dye molecules on the photocatalyst surface.

3.3. Degradation studies of IC/NP under UV/solar light

Degradation of IC is insignificant in the absence of TiO_2 and no degradation occurs in the absence of light when TiO_2 is present. Thus the decrease in the concentration of dye molecules arises from the photocatalytic activity of excited semiconductor. A series of experiments were performed and the photocatalyst dosage was optimized at 300 mg and dye concentration was optimized at 100 ppm for IC. Table 1 shows the percentage degradation of IC catalyzed by various photocatalysts under UV/solar irradiation. An initial 38% and 7% decrease in the concentration of IC was observed under UV and solar illumination respectively with bare TiO_2. The degradation was stronger at acidic pH 4.5 and was found to decrease with increase in pH of the solution. The point of zero charge (pzc) of TiO_2 is widely reported to be as pH ~6.25. Thus surface charge density remains positive below pzc, while remains negative above it. The negatively charged sulfonate group drives the IC molecule to get strongly adsorbed on the TiO_2 surface at acidic pH 4.5 (Fig. 7). The stronger preadsorption of pollutant molecule enhances the degradation rate due to efficient charge transfer between the photocatalyst surface and the dye molecule. Under alkaline conditions, surface charge remains negative which exert columbic repulsion for the dye molecules resisting its adsorption, which obviously results in lower activity. Hence all the photocatalytic experiments were performed at pH 4.5. Dyes can be degraded under visible irradiation via two competitive processes: photocatalytic processes and self photo sensitized process. Thus it is very difficult to differentiate the degradation mechanism and also the photocatalyst efficiency. Hence to exclude the effect of self-photosensitzation and confirm whether prepared photocatalysts is photoactive under solar light illumination, we evaluated the photocatalytic activity for the degradation of 20 ppm NP under UV/solar light (Fig. 8). The degradation of NP under solar light with TiO_2 is almost negligible since it cannot be activated under visible light due to its large band gap, while the metal ion doped catalysts showed higher activity compared to undoped titania. To quantitatively understand the reaction kinetics of pollutant degradation, we analyzed the degradation data with the pseudo-first-order kinetic

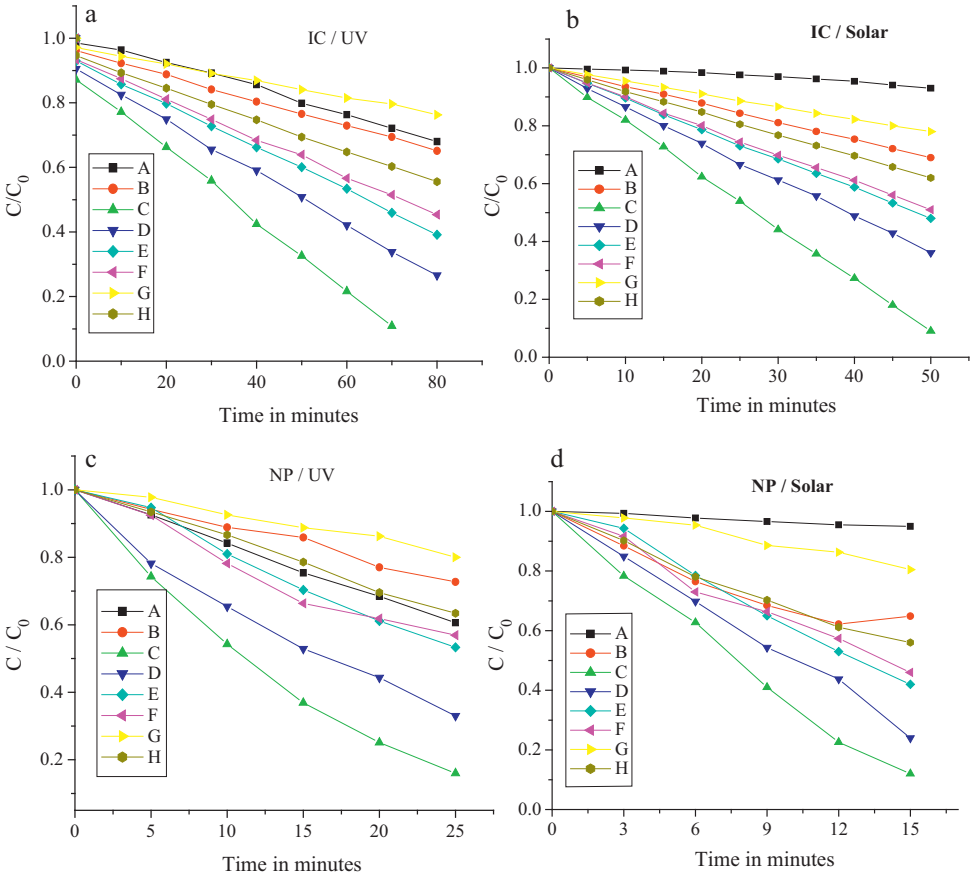

Fig. 8. Degradation profile of IC (a and b)/NP (c and d) under UV and solar light illumination using various photocatalysts at optimum dopant concentration. (A) TiO_2; (B) V^{5+}-TiO_2; (C) Mn^{2+}-TiO_2; (D) Fe^{3+}-TiO_2; (E) Ru^{3+}-TiO_2; (F) Os^{3+}-TiO_2; (G) Ni^{2+}-TiO_2; (H) Zn^{2+}-TiO_2.

model, which is generally used for the photocatalytic degradation, if the initial concentration of the pollutant is low:

$$\ln\left(\frac{C}{C_0}\right) = -kt \quad (3)$$

where C_0 and C are the concentration of the dye in solution at time 0 and t, respectively and k is the pseudo-first-order rate constant. The rate constant calculated from the data are plotted and shown in Fig. 8 and the results are summarized in Table 2. The rate constant calculated for Mn^{2+} (0.06 at.%)-TiO_2 is 3.6 times higher than the undoped TiO_2 and 1.8 times higher than that of Fe^{3+} (0.06 at.%)-TiO_2 for NP degradation under UV light. Similar comparison can be made for IC degradation among the various catalysts. For both the pollutants, the photocatalytic efficiency was higher under solar light compared to UV light illumination. This might be due to the fact that intermediates formed during the course of the degradation reaction were destroyed at a faster rate under solar light. Moreover, under UV light, band gap excitation involves only the transfer of electrons from valence band to conduction band and the electronic level of the dopant serve predominantly as trapping site for the charge carriers. Liu et al. suggested that the existence of I–O–Ti just above the valence band and I–O–I below the conduction band gives rise to favorable surface structure resulting in excess generation of hydroxyl radicals in iodine doped titania [30e]. Li et al. found that Nd^{3+} substituting Ti^{4+} lattice sites in TiO_2 matrix introduces electronic states into the band gap of TiO_2 to form new lowest unoccupied molecular orbital [64b]. In the line of these arguments, we speculate that occupied states M–O–Ti just above the valence band edge and unoccupied states M–O–M structure below the conduction band edge might be formed due to the substitution of metal ion dopant 'M' in Ti–O–Ti framework. Under these situations, the transition takes place in several ways: (i) occupied states to conduction band; (ii) valence band to the unoccupied states; (iii) valence band to oxygen vacancy states and so on under solar light (Fig. 9). It should be noted that lower valent cations creates an oxygen vacancies in the neighboring co-ordination sphere for charge compensation. Thus extrinsic absorption involving oxygen vacancies, surface states and other defect centers induced by the dopants within the TiO_2 matrix under visible light irradiation results in the dense generation of charge carriers compared to UV light irradiation. Furthermore, the unoccupied states M–O–M serves as efficient electron traps, while occupied states M–O–Ti acts as hole trap increasing the overall efficiency. This might result in higher activity for doped catalyst under solar light compared to UV light.

Table 2
Rate constant (10^{-2} min^{-1}) calculated from the plot of $-\log C/C_0$ versus time for NP and IC degradation under UV/solar light illumination.

TiO_2	Rate constant for NP degradation		Rate constant for IC degradation	
	UV	Solar	UV	Solar
TiO_2	2.10	0.27	0.47	–
V^{5+} (0.06%)-TiO_2	1.32	2.57	0.48	0.75
Mn^{2+} (0.06%)-TiO_2	7.68	15.91	2.77	4.61
Fe^{3+} (0.06%)-TiO_2	4.23	9.98	1.49	2.03
Ru^{3+} (0.06%)-TiO_2	2.86	6.70	1.05	1.48
Os^{3+} (0.06%)-TiO_2	2.41	5.39	0.90	1.35
Ni^{2+} (0.08%)-TiO_2	0.94	1.63	0.29	0.50
Zn^{2+} (0.06%)-TiO_2	1.99	3.99	0.66	0.96

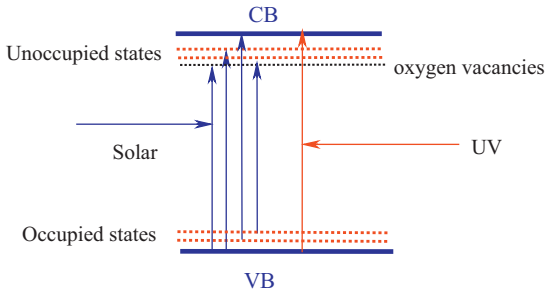

Fig. 9. Energy levels representing the UV and visible transition in transition metal ion doped TiO_2 photocatalyst. Red and blue color arrows indicate transition takes place in UV and solar light illumination respectively. Black dotted line corresponds to oxygen vacancy band and red color line indicates the energy level of dopant either below the conduction band (unoccupied states) or above the valence band edge (occupied states). (For interpretation of the references to colour in this figure legend, the reader is referred to the web version of the article.)

3.4. Influence of physicochemical–electronic properties of transition metal ion doped titania on photocatalytic activity

A general photochemical charge trapping, recombination, detrapping and migration mechanism in the presence of metal ion dopants can be proposed as follows [15]:

Charge carrier generation:

$$M^{n+} + h\nu \rightarrow M^{(n+1)+} + e^-_{cb} \quad (4)$$

$$M^{n+} + h\nu \rightarrow M^{(n-1)+} + h^+_{vb} \quad (5)$$

Charge trapping:

$$Ti^{4+} + e^- \rightarrow Ti^{3+} \quad (6)$$

$$M^{n+} + e^- \rightarrow M^{(n-1)+} \quad (7)$$

$$M^{n+} + h^+ \rightarrow M^{(n+1)+} \quad (8)$$

$$> OH^- + h^+ \rightarrow OH^\bullet \quad (9)$$

Charge release and migration:

$$Ti^{4+} + M^{(n-1)+} \rightarrow Ti^{3+} + M^{n+} \quad (10)$$

$$M^{(n+1)+} + > OH^- \rightarrow M^{n+} + OH\cdot \quad (11)$$

Recombination:

$$e^- + h^+ \rightarrow \text{heat} \quad (12)$$

$$Ti^{3+} + > OH^\bullet \rightarrow Ti^{4+} + > OH^- \quad (13)$$

$$M^{(n-1)+} + h^+ \rightarrow M^{n+} \quad (14)$$

$$M^{(n-1)+} + > OH^\bullet \rightarrow M^{n+} + > OH^- \quad (15)$$

$$M^{(n+1)+} + e^- \rightarrow M^{n+} \quad (16)$$

$$M^{(n+1)+} + Ti^{3+} \rightarrow M^{n+} + Ti^{4+} \quad (17)$$

Interfacial charge transfer process:

$$e^- (\text{or } Ti^{3+},\ M^{(n-1)+}) + O \rightarrow O^- \quad (18)$$

$$h^+ \quad (\text{or} > OH^\bullet,\ M^{(n+1)+}) + R \rightarrow R^+ \quad (19)$$

M^{n+} is metal ion dopant, O is an electron acceptor (oxidant) and R is an electron donor (reductant).

The dopant inside the TiO_2 matrix determines the formation of permanent space charge region whose potential drives the electron–hole separation and consequently results in the charge transfer from $-O-Ti^{4+}$ to $-^\bullet O-Ti^{4+}$. M^{n+}-TiO_2 (M^{n+} = Mn^{2+}, Fe^{3+}, Ru^{3+} and Os^{3+}) photocatalysts showed significant enhancement in the degradation rate for both the substrates, while photoactivity of V^{5+}-TiO_2, Ni^{2+}-TiO_2 and Zn^{2+}-TiO_2 were found to be less or almost equal to TiO_2 under UV light. Since the photocatalysts were excited under equal absorption conditions, the lower or almost equal reactivity of V^{5+}-TiO_2, Ni^{2+}-TiO_2 and Zn^{2+}-TiO_2 compared to TiO_2 can only originate from the electronic structure of doped samples. The trapped charge carriers in the localized level of dopant can react with free charge carriers resulting in recombination; the free hole can recombine with trapped electron or a free electron can recombine with trapped hole which can significantly nullify the dopant effects. All the metal ion doped titania showed maximum activity at a dopant concentration of 0.06 at.% excluding for Ni^{2+}-TiO_2, which showed enhanced activity at a dopant concentration of 0.08 at.%, which suggests that relatively small amounts of dopant inside the TiO_2 matrix can act as a electron or hole trapping site and inhibits the recombination of charge carriers and prolongs their lifetime. Pleskov reported that the value of space charge region potential for the effective separation of photogenerated charge carriers must not be lower than 0.2 eV [65]. On the other hand, the thickness of space charge layer is influenced by the dopant concentration according to the following Eq. (20)

$$W = \left(\frac{2\varepsilon\varepsilon_0 V_S}{eN_d}\right)^{1/2} \quad (20)$$

where 'W' is the thickness of space charge layer, ε and ε_0 are the static dielectric constants of the semiconductor and of the vaccum, V_s is the surface potential, N_d is the number of dopant donor atoms, e is the electronic charge. The above equation clearly shows that W decreases as the dopant content increases [66]. In addition, penetration depth l, of the light into the solid is given by $l = 1/a$, in which 'a' is the light absorption coefficient at a given wavelength. When the value of W approximates that of l, all the photons absorbed generates electron–hole pairs that are efficiently separated. Consequently, it is understandable that the existence of optimum value of N_d for which a space charge region exist whose potential is not less than 0.2 eV and whose thickness is more or les equal to light penetration depth [66]. In the present case, optimum value of N_d approximates to that of 0.08 at.% for Ni^{2+} and 0.06 at.% for other metal ions in the TiO_2 lattice. For higher dopant concentration (0.1 at.%), the space charge region may become narrow and the penetration depth of light into TiO_2 greatly exceeds the thickness of the space charge layer. The charge carriers thus generated are field free and hence recombine rapidly. Also, the high concentration of the dopants can steadily become the recombination sites for the charge carriers evidently decreasing the photocatalytic activity.

Irrespective of excitation source and nature of substrate chosen, photocatalytic activities of for various doped photocatalysts followed the order: Mn^{2+}-TiO_2 > Fe^{3+}-TiO_2 > Ru^{3+}-TiO_2 ≥ Os^{3+}-TiO_2 > Zn^{2+}-TiO_2 > V^{5+}-TiO_2 > Ni^{2+}-TiO_2 at an optimum dopant concentration in the TiO_2 matrix (Table 2). The transition metal ion dopant within the TiO_2 matrix can intrinsically alter the electronic structure and consequently the absorbance, redox potential and charge-carrier mobility of the semiconductor photocatalyst. Many parameters affects the reactivity of a photocatalytic system such as electronic properties of the semiconductor (band gap absorption, relative position of valence and conduction band edges, position of dopant electronic level), separation efficiency of photogenerated charge carriers, light absorption coefficient, nature of interface, dopant electronic configuration and physical variables like surface area, crystallite size, surface structure, dopant concentration, and on the surface morphology etc.

Wold et al. found a relationship between the surface acidity of WO_3/TiO_2 and MoO_3/TiO_2 and their relative photo efficiencies [67]. For these systems, the increase in the surface acidity was directly proportional to the amount of higher valent transition metal ion. In the line of these arguments, V^{5+}-TiO_2 samples is expected to possess higher surface acidity than other photocatalysts. V^{5+}-TiO_2 showed higher adsorptive capacity for IC owing to its higher surface

Table 3
Percentage of initial adsorption of IC on various photocatalyst surface.

Photocatalysts	Percentage adsorption
TiO_2	5.5
V^{5+} (0.10%)-TiO_2	12.5
Mn^{2+} (0.10%)-TiO_2	4.5
Fe^{3+} (0.10%)-TiO_2	10
Ru^{3+} (0.10%)-TiO_2	10
Os^{3+} (0.10%)-TiO_2	10
Ni^{2+} (0.10%)-TiO_2	9.5
Zn^{2+} (0.10%)-TiO_2	9.0

acidity, yet resulted in lower activity (Table 3). The high adsorption of pollutants although proved to enhance photocatalytic activity [52], was not a beneficial factor in the present study. Another possible explanation is that the higher amount of pollutant adsorption can prevent the photoexcitation of semiconductor itself and it can also serve as inner filter which can prevent the photons reaching the catalyst surface reducing the concentration of free radicals in the solution.

It is well known that the photoreactivity also depends on the concentration of surface adsorbed water molecules and hydroxyl anions on the titania surface. Since the dopants excluding V^{5+}, were lower valent than the host Ti^{4+} ions, decrease in the concentration of surface adsorbed water molecules were observed, although the bands were slightly broadened due to the smaller crystallite size of the samples [68]. V^{5+}-TiO_2 samples, showed no significant reduction in the crystallite size of the samples, but there was drastic increase in the concentration of surface adsorbed water molecules as confirmed FTIR analysis. The dopant V^{5+} being hypervalent than the host Ti^{4+}, it attracts additionally one hydroxyl anions for charge compensation [69]. However, concentration of adsorbed water molecules as measured by FTIR spectroscopy for all the photocatalysts did not have any relationship on the photocatalytic activity in the present study. In any photocatalytic processes, the surface adsorbed water and hydroxyl groups can only be the potential sites to trap the holes on the surface, but the final hole transfer to surface adsorbed species critically needs favorable surface structure. Hence we speculate that the lack of surface structure in V^{5+}-TiO_2 samples resulted in lower activity.

The surface area for most of the doped samples was higher than Mn^{2+}-TiO_2 doped samples. Larger surface area may be an important factor for the photocatalytic degradation reactions, as large amount of pollutant can be adsorbed promoting the interfacial charge transfer rate. However the photocatalysts with larger surface area is usually associated with large amount of crystalline defects favoring the recombination of electron-hole pairs leading to low photocatalytic activity. Hence larger surface area is a requirement but cannot be a decisive factor in many cases [70].

Although the metal ion doped titanates enhanced the intensity of fundamental absorption edge of TiO_2 and extended its band gap absorption to the visible region, there exists no direct correlation between either of two on photocatalytic activity. Fe^{3+}-TiO_2, Ru^{3+}-TiO_2, Os^{3+}-TiO_2 and Ni^{2+}-TiO_2 doped samples showed large shift in the band gap absorption compared to Mn^{2+}-TiO_2 but resulted in lower photocatalytic activity. It is commonly accepted that narrower band gap corresponds to less powerful redox ability, since the photocatalytic system can be assumed to be an electrochemical cell, the large decrease in the band gap results in lower oxidation–reduction potential based on the Eq. (21)

$$\Delta G = -nFE \tag{21}$$

ΔG is the free energy change of the redox process occurring in the system, n is the number of electrons involved in the redox process, F is the Faraday constant and E represents the band gap energy of the semiconductor. This indicates that the large band gap narrowing in the case of Fe^{3+}-TiO_2, Ru^{3+}-TiO_2, Os^{3+}-TiO_2 and Ni^{2+}-TiO_2 could be unfavorable for the photocatalytic activity under UV light [71].

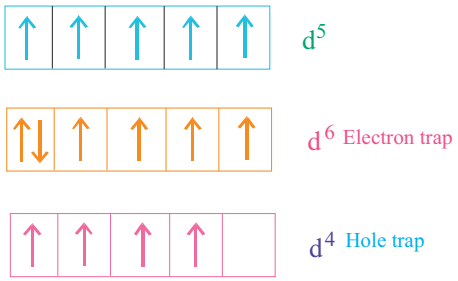

Fig. 10. Electron/hole trap for the metal ion having half filled electronic configuration as per Ref. [17b].

Choi et al. suggested that the photoreactivity of doped TiO_2 materials appears to be complex function of energy level of dopant within the TiO_2 lattice, their d electronic configuration and the distribution of dopants [15]. According to the energy level of dopant within the TiO_2 matrix depicted based on the band gap absorption in the visible region of the doped samples, the electronic energy level of dopants Fe^{3+}, Ru^{3+}, Os^{3+} and Ni^{2+} forms a mid bandgap states which can serve as both electron and hole traps, while dopants Mn^{2+}, V^{5+} and Zn^{2+} serve predominantly as electron traps as their localized electronic level is just below the conduction band edge. Also, the chances of holes reaching the localized electronic level of these dopants are too less, since they can be trapped by hydroxyl anions or pollutant molecules adsorbed on the surface before they can reach the dopant level. Since V^{5+} has vacant 'd' orbital, its probability to serve as hole trap will be minimum, while Zn^{2+} has completely filled 'd' orbitals, its role as an electron trap will be negligible. Hence it can be speculated that V^{5+} and Zn^{2+} can serve mainly as electron and hole trap respectively. The dopants should serve as both electron and hole traps to be highly photoactive. Trapping either an electron or hole alone is ineffective because the immobilized charge species quickly recombines with its mobile counterpart [15].

Mn^{2+} and Fe^{3+}, Ru^{3+}, Os^{3+} has valence electronic configuration of $3d^5$, $4d^5$ and $5d^5$, respectively. When these dopant ions trap electron/hole, there will be considerable loss of spin energy due to the change in electronic configuration from d^5 (half filled high spin) to low spin d^6/d^4 (electron/hole trap). According to crystal field theory, since both the spin states are highly unstable, the trapped electron/hole will be transferred to surface adsorbed oxygen/surface adsorbed water molecules or hydroxyl groups to restore its spin energy thereby suppressing the recombination reaction (Fig. 10). According to the literature, Fe^{3+} and Mn^{2+} have feasibility of serving as effective charge carrier traps [15,17,53,61a]. Even though, Mn^{2+} and Zn^{2+} has similar oxidation state, almost identical band gap absorption and stable electronic structures, their influence on photocatalytic activity was substantially different.

Since most of the doped photocatalysts showed only anatase phase, their efficiency for the degradation of IC and NP were different under UV/solar light over the entire range of dopant concentration. The enhanced activity of Mn^{2+}-TiO_2, Fe^{3+}-TiO_2, Ru^{3+}-TiO_2 and Os^{3+}-TiO_2 samples compared to others can be critically attributed to stable unique half filled electronic configuration of these dopants, which is in accordance with previous reports [15,17,52–54]. However, at a dopant concentration of 0.02 at.%, only Mn^{2+}-TiO_2 samples showed enhanced activity compared to Fe^{3+}-TiO_2, Ru^{3+}-TiO_2 and Os^{3+}-TiO_2 samples, despite the fact that all the photocatalyst exhibited anatase phase and all the dopants had half filled electronic configuration. Murakami et al. [16], studied the photocatalytic activity of TiO_2 modified by Fe^{3+}, Cu^{2+}, Ni^{2+} and Cr^{3+} ions for the oxidation of acetaldehyde. The order of activity was

found to be $Fe^{3+} > Cu^{2+} > Ni^{2+} > Cr^{3+}$ which was well in agreement with their standard positive reduction potentials. Accordingly, Fe^{3+} served as better electron acceptor owing to its higher positive reduction potential which resulted in the high photocatalytic activity for Fe^{3+}-TiO_2 sample. Similar trend was also observed even in the present research work. The standard redox potential for Mn^{2+}/Mn^{3+}, Fe^{3+}/Fe^{2+}, Ru^{3+}/Ru^{2+} and Os^{2+}/Os^{3+} redox pairs are 1.56, 0.77, 0.24 and 0.26 V, respectively [72–74]. Hence it can be concluded that Mn^{2+} serves as efficient charge carrier traps for the photogenerated charge carriers compared to Fe^{3+}, Ru^{3+} and Os^{3+} ions, although all these dopants possess half filled electronic structure. The reduction potential of V^{5+}/V^{4+}, Ni^{2+}/Ni and Zn^{2+}/Zn are 0.06, −0.24 and −0.76 V, respectively [75,16]. But the photocatalytic activity followed the order Zn^{2+}-$TiO_2 > V^{5+}$-$TiO_2 > Ni^{2+}$-TiO_2, which was not in agreement with the works of Murakami et al. [16]. In our previous research work [57a], we showed enhanced activity of Zn^{2+}-TiO_2 compared to V^{5+}-TiO_2 due to the stable filled electronic configuration of Zn^{2+} ion and also to smaller crystallite size of the Zn^{2+}-TiO_2 samples compared to V^{5+}-TiO_2. Volume recombination of charge carrier prevails over interfacial charge transfer processes in the large crystallites of V^{5+}-TiO_2 compared to other doped samples [57a]. The lowest activity of Ni^{2+}-TiO_2 compared to other doped catalysts may be probably due to deleterious bulk recombination of charge carriers due to the dopant level acting as recombination centers and the induced localized states may not be optimal to facilitate photooxidation reactions. Another plausible speculation is that the Ni^{2+} with partially filled electronic configuration might result in deep trap of the charge carriers rather than the shallow traps, consequently resulting in decreased activity.

At this stage, we would like to emphasize that the general consideration made so far according to the available literature is not sufficient to predict a good dopant. However, an attempt is made to find a new set of parameters that can critically influence the photocatalytic activity. These findings suggests that crucial parameters like large surface area, smaller crystallite size, narrow band gap, higher amount of pollutant adsorption, anatase phase, unique half filled electronic structure of the dopant which was found to influence the photocatalytic activity could not be correlated with enhanced activity of Mn^{2+} (0.06 at.%)-TiO_2. Hence it is suggested that the photocatalytic activity of metal ion doped titania is a complex function of several physicochemical–electronic properties.

The high photocatalytic activity of Mn^{2+} (0.06 at.%)-TiO_2 was attributed to synergistic effect in the bicrystalline framework of anatase and rutile. It is well known that TiO_2 with bicrystalline framework of anatase–rutile or rutile–brookite or anatase–brookite can effectively reduce the recombination of photogenerated charge carriers and thereby enhances the photocatalytic activity [76–114]. It is commonly accepted that anatase polymorph exhibits superior activity compared to rutile polymorph. The different behavior of rutile and anatase were initially attributed to difference in the position of conduction band (more positive for rutile with respect to NHE). Anatase has inherent surface band bending that is spontaneously formed in deeper region with steeper potential in comparison with rutile. In anatase, surface hole trapping dominates because the spatial charge separation is achieved by the migration of photogenerated holes towards the particle surface due to strong upward band bending. In rutile, bulk generated charge carriers prevail since only the holes sufficiently close to the surface migrate before recombination [115]. However, in the mixed phase, one of the phase sensitizes the photoinduced electron transfer to the other phase depending on the relative position of conduction and valence band edges. Thus solid–solid interface between the two phases is a key structural feature that facilitates charge separation to suppress recombination which may be due to the locus of defect sites acting as catalytic hot spots. Compared to pure phases, the mixed phase TiO_2 materials have unique charge transfer and recombination dynamics, fast diffusion of charge carriers to the surface or interface that accelerates the interfacial charge transfer processes [115].

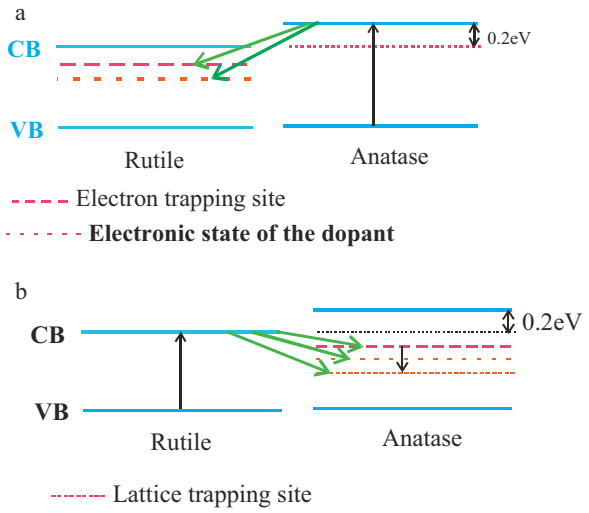

Fig. 11. (a) Vectorial interparticle electron transfer in the mixed phase under UV light. (b) Vectorial interparticle electron transfer in the mixed phase under solar light.

Serpone et al. suggested that trapped charge carriers dictates the redox reactions rather than free charge carriers as they undergo recombination much faster than the trapped ones [116]. Hence the fate of hydroxyl radical generation which is critical for degradation reactions depends on the interfacial charge transfer mechanisms. The bicrystalline framework with high intimate contact in Mn^{2+}-TiO_2 sample along with unique half filled electronic configuration of Mn^{2+} and high standard reduction potential of Mn^{2+}/Mn^{3+} pairs accelerates the interfacial charge transfer process leading to the enhanced generation of hydroxyl radicals under UV/solar light, which obviously results in higher reaction rates. In the mixed-phase of anatase and rutile, photogenerated hole and electron preferentially gets trapped on O^- and Ti^{3+} centers of the rutile phase, even when anatase is the main component [117]. Under UV excitation, anatase in the mixed phase gets activated as it is a good absorber of UV light photons (Fig. 11a). This indicates that electron transfer occurs from the higher energy conduction band states of anatase to those of rutile at lower energy and simultaneously hole transfer occurs from the lower energy valence band states of anatase to those of rutile at higher energy. Thus rutile serves as passive electron sink hindering the recombination in anatase phase [118]. Subsequent electron transfer from rutile trapping site to the impurity level further favors the charge separation [119], which accounts for superior activity of Mn^{2+} (0.06 at.%)-TiO_2.

The band gap of rutile is favorable for visible light excitation as the conduction band edge of rutile lies 0.2 eV below the conduction band edge of anatase. Under visible light excitation, the photogenerated electron from conduction band of rutile transfers to trapping sites of anatase phase which can be considered as antenna effect by rutile phase [120]. Subsequent electron transfer to lattice trapping sites of anatase or to localized level of dopant further separates the charge carriers effectively (Fig. 11b). The lattice trapping sites of anatase has energy of 0.8 eV less than the anatase conduction band edge [121]. Thus by competing with the recombination, the charge separation activates the photocatalyst and the hole originating from the rutile valence band participates in the oxidative degradation of organic pollutants.

In order for such a vectorial interparticle electron transfer to be possible, the two crystalline polymorphs must be in close contact. The intimate contact between the two polymorphs depends on

their crystallite size. Hong et al. reported that iodine-doped titania with mixed phases of anatase and rutile showed lower activity compared to iodine-doped anatase titania [122]. The low activity was due to the large rutile crystal size which resulted in poor intimate contact between these two phases which failed to demonstrate its structure advantage. Mixed phase of anatase and rutile were also obtained by doping Fe^{3+}, Cr^{3+} and Co^{2+} into TiO_2 matrix prepared by sol–gel route in the presence of surfactant which showed lower activity compared to pure TiO_2 [123]. However, the authors suggested that only Co^{2+} induces phase transformation from anatase to rutile, while mixed phase in Fe^{3+} and Cr^{3+} doped TiO_2 photocatalysts is due to loss of crystallinity. In the present case, Mn^{2+} ion induces phase transformation from anatase to rutile without the formation of any secondary oxides, which accounts for the difference in photoreactivity of doped samples with mixed phases compared to other research groups. Hence it is crucial to maintain the crystallite size of both the polymorphs for intimate contact, which enables the mixed phase for efficient charge transfer. Since the crystallite size of both the phases are same in Mn^{2+} (0.06 at.%)-TiO_2, it can be speculated that both anatase and rutile polymorph are in intimate contact. According to Gray's results, such an interfacial mixed polymorph structure would contain a surplus amount of tetrahedral Ti^{4+} sites which can act as reactive electron-trapping sites [124]. The isolated tetrahedral Ti^{4+} sites are more active than octahedrally coordinated Ti^{4+} sites as in bulk TiO_2. These tetrahedral Ti^{4+} sites could serve as catalytic hot spots at anatase/rutile interface and thus avails the mixed polymorph nanocrystals into an effective photocatalytic relay for solar energy utilization [124]. Hence we believe that these tetrahedral Ti^{4+} sites contribute to the increased activity of the mixed phase relative to the pure anatase phase. The small crystallite size in Mn^{2+} (0.06 at.%)-TiO_2 sample reduces the diffusion path length for the charge carriers, from the site where they are photoproduced to the site where they react. Reduction in this diffusion path length results in reduced recombination of charge carriers resulting in enhanced interfacial charge transfer process. Therefore such an intimate contact between the mixed polymorph with smaller crystallite will have a core of rutile crystallites interwoven with bound anatase crystallites, thus accelerating the transfer of electrons from rutile to neighbouring anatase sites or to the impurity level created by the dopant.

At dopant concentration around 0.1 at.%, the crystallite size for both the phases is found to be 16.6 nm in Mn^{2+}-TiO_2 sample. Most of the charge carriers in these crystallites are generated sufficiently close to the surface. As a result, the photogenerated charge carriers may quickly reach the surface resulting in faster surface recombination reaction. This is also due to the excess trapping sites in the sample and the lack of driving force to separate these charge carriers. In the photocatalyst with smaller crystallite size, surface charge carrier recombination outweighs the interfacial charge transfer process. Since Mn^{2+} serves as trapping site for both electron and hole, the possibilities of trapping these charge carriers will be high at higher dopant concentration and this trapped charge carrier pair may recombine through quantum tunneling. Moreover, at a high dopant concentration, the charge carriers may be trapped more than once on its way to the surface so that their mobility becomes extremely low and undergoes recombination before it can reach the surface [125]. Therefore there is a need for optimal dopant concentration in the TiO_2 matrix to get effective crystallite size for highest photocatalytic efficiency. Beyond the optimum dopant concentration, the rate of recombination starts dominating the reaction in accordance with the Eq. (22)

$$K_{RR}\alpha \exp\left(\frac{-2R}{a_0}\right) \tag{22}$$

where K_{RR} is the rate of recombination, R is the distance separating the electron and hole pairs, a_0 is the hydrogenic radius of the wave function for the charge carrier. As a consequence the recombination rate increases exponentially with the dopant concentration because the average distance between the trap sites decreases with increasing number of dopant confined within a particle [15,126]. The similar line of reasoning holds well towards the lower activity for other doped samples at high dopant concentration (≥0.1 at.%).

The existence of optimum rutile fraction to enhance the activity of mixed phase was recently explained using a new model based on band gap configuration in the connected nanocrystallite as a function of size distribution and phases involved by Zachariah et al. [105]. It is assumed that the nanocrystalline anatase TiO_2 is made up of broad nanocrystalline size distribution and the band gap of anatase TiO_2 increases below the critical size. Hence, if the nanoparticle distribution is below the critical size, then the band gap of connected nanocrystallite would be different depending on their size. In the light of this model, we would speculate that the electronic interaction between the anatase and rutile leads to spatial charge separation, while the nanocrystallite located at the centre would serve as both sink and source for hole and the localized band of Mn^{2+} within the TiO_2 matrix would serve as charge carrier trap, which would obviously lead to enhanced activity. With increase in rutile fraction in the mixed phase, more number of contacts would be established between rutile–rutile crystallite having identical band gap, leading to the decrease in photocatalytic activity [105].

We have also prepared mixed phase of anatase and rutile by physically grinding the pure anatase and rutile in the ratio 90:10 and also by simple hydration–dehydration cycle. The rutile crystallite was ~40 nm obtained by calcining the sample at 700 °C. However, the interface obtained by the physical mixing of anatase and rutile phase powders resulted in very poor activity compared to pure anatase TiO_2 itself (data not shown). The interface obtained by random collisions and also the large particle size of rutile resulted in poor charge transfer between the mixed phases. The mixed phase powders prepared by hydration–dehydration cycle showed considerably enhanced activity relative to pure phases suggesting that electronic interaction and the intimate contact between the mixed phases is crucial to show synergy. However, the activity was still lower compared to Mn^{2+} (0.06 at.%)-TiO_2 indicating that dopant Mn^{2+} inside TiO_2 matrix additionally contributed to overall efficiency. These results suggests that chemical contact between heterophases prepared by in situ via calcination in the present study had steadier and tighter interfaces to enhance charge transfer and also avoids self agglomeration of two polymorphs.

In any case, it is vital that the existence of synergistic effect between the mixed polymorphs is not universal [127], and there exist an optimum value for both the phases to show enhanced activity. In the present case, optimum value of anatase:rutile ratio is 90:10. The optimum rutile fraction in the mixed phase to enhance the photocatalytic activity as reported by several research groups is shown in Table 4. The present research probably report the lower rutile fraction in the mixed phase to show the enhance activity, which is even lower than the benchmark photocatalyst Degussa P25. The expansion in the crystal matrix due to Mn^{2+} doping induces oxygen vacancies in the neighboring co-ordination sphere, which generates shallow energy states at the bottom of the conduction band and served as electron trap site in nanocrystalline TiO_2 [128].

$$MnO \leftrightarrow Mn''_{Ti} + Oo + Vo^{\bullet\bullet}/2Vo^{\bullet} \tag{22}$$

$$Vo^{\bullet\bullet} + e^- \rightarrow Vo^{\bullet} \tag{23}$$

$$Vo^{\bullet} + O_2 \rightarrow Vo^{\bullet\bullet} + {O_2}^{-\bullet} \tag{24}$$

Meanwhile, shallow energy states introduced by metal ion at the top of valence band served as hole trap sites [129]. The separation of the charge carriers is attributed to such trapping. Subsequently,

Table 4
Optimum rutile content in the mixed phase titania showing enhanced photoactivity as reported by several research groups.

Research group	Optimum rutile content (wt.%)	Reference
Panpranoat et al.	44	[76]
Meulen et al.	20	[77]
Basca and Kiwi	30	[78]
Lei and Duan	40	[80]
Lopez et al.	08	[83]
Jung et al.	11	[85]
Bessekhouad et al.	12.5	[86]
Xiao et al.	51.61	[87–89]
Zhao et al.	33	[90]
Yan et al.	25.8	[92]
Li et al.	3.6	[99]
Xu and Zhang	62	[101]
Liu et al.	43	[102]
Chen et al.	30	[104]
Zachariah et al.	40	[105]
Kolenkao et al.	15	[107]
Bakardjieva et al.	22.6	[108]
Chen et al.	28	[109]
Chan et al	42	[110]
Jongsomjit et al.	19	[111]
Chen et al.	18	[113]

the charge carriers get transferred to the surface of photocatalyst and participate in the redox reactions. Thus the distortion induced by Mn^{2+} doping in TiO_2 lattice gives higher surface energy than pure TiO_2 which effectively reduces the recombination between electron–hole pairs, enhancing the interfacial energy transfer process. In conclusion, the order of reactivity of the various transition metal ion doped titania for the degradation of IC/NP are satisfactorily explained based on the obtained results and more intensive study is needed in order to depict the exact role of dopant inside TiO_2 matrix. The photocatalytic activity of the doped titania is a complex function of several physicochemical–optical parameters and it is rather difficult to assess individual contribution from each one of them. Although intense research is devoted to metal ion doped TiO_2, it is rather difficult to make unified decision and the role of dopant inside the TiO_2 matrix still remains elusive.

4. Conclusion

In order to provide a deep insight on the influence of physicochemical–electronic properties of semiconductor photocatalyst on photocatalytic activity, anatase TiO_2 was doped with several transition metal ions like V^{5+}, Mn^{2+}, Fe^{3+}, Ru^{3+}, Os^{3+}, Ni^{2+} and Zn^{2+} having vacant, half, partially and completely filled 'd' orbital. All the dopants stabilized anatase phase, excluding Mn^{2+} which promoted the phase transformation from anatase to rutile when the samples calcined at 550 °C. The photocatalytic activities of these photocatalysts were evaluated for the degradation of IC and NP under UV/solar light. The experimental results suggest that crucial parameters like large surface area, smaller crystallite size, narrow band gap, higher amount of pollutant adsorption, anatase phase, unique half filled electronic structure of the dopant which was found to influence the photocatalytic activity according to the literature, could not be correlated with enhanced activity of Mn^{2+} (0.06 at.%)-TiO_2. The enhanced activity of Mn^{2+} (0.06 at.%)-TiO_2 was thus attributed to the combined effects of (i) synergistic effects in the bicrstalline framework of anatase and rutile which involves vectorial interparticle electron transfer; (ii) high positive reduction potential of Mn^{2+}/Mn^{3+} pairs; (iii) optimum rutile content with high intimate contact between the crystallites of the mixed phases; (iii) Favorable surface structure with high lattice and surface energy which transfer the hole to surface adsorbed water or hydroxyl groups; (iv) induced oxygen vacancies which form a shallow energy states at the bottom of the conduction band acting as reactive electron trapping site.

References

[1] A. Fujishima, K. Honda, Nature 238 (1972) 37–38.
[2] X. Zhu, J. Zhang, F. Chen, Chemosphere 78 (2010) 1350–1355.
[3] A.G.S. Prado, L.B. Bolzon, C.P. Pedroso, A.O. Moura, L.L. Costa, Appl. Catal. B: Environ. 82 (2008) 219–224.
[4] A. Ishikawa, T. Takata, J.N. Kondo, M. Hara, H. Kobayashi, K. Domen, J. Am. Chem. Soc. 124 (2002) 13547–13553.
[5] L. Zhang, W. Wang, J. Yang, Z. Chen, W. Zhang, L. Zhou, S. Liu, Appl. Catal. A: Gen. 308 (2006) 105–110.
[6] H. Fu, J. Lin, L. Zhang, Y. Zhu, Appl. Catal. A: Gen. 306 (2006) 58–67.
[7] J. Yu, J. Xiong, B. Cheng, Y. Yu, J. Wang, J. Solid State Chem. 178 (2005) 1968–1972.
[8] H. Kato, A. Kudo, Catal. Lett. 58 (1999) 153–155.
[9] J. Tang, Z. Zou, J. Ye, Chem. Mater. 16 (2004) 1644–1649.
[10] X.F. Cheng, W.H. Leng, D.P. Liu, J.Q. Zhang, C.N. Cao, Chemosphere 68 (2007) 1976–1984.
[11] (a) F. Han, V.S.R. Kambala, M. Srinivasan, D. Rajarathnam, R. Naidu, Appl. Catal. A: Gen. 359 (2009) 25–40;
(b) J. Yu, H. Yu, B. Cheng, C. Trapalis, J. Mol. Catal. A: Chem. 249 (2006) 135–142;
(c) J. Yu, X. Zhao, Q. Zhao, Mater. Chem. Phys. 69 (2001) 25–29;
(d) H. Yu, J. Yu, B. Cheng, J. Lin, J. Hazard. Mater. 147 (2007) 581–587;
(e) J. Yu, Y. Su, B. Cheng, M. Zhou, J. Mol. Catal. A: Chem. 258 (2006) 104–112;
(f) J. Yu, G. Wang, B. Cheng, M. Zhou, Appl. Catal. B: Environ. 69 (2007) 171–180;
(g) J. Yu, S. Liu, H. Yu, J. Catal. 249 (2007) 59–66.
[12] (a) J. Yu, X. Yu, B. Huang, X. Zhang, Y. Dai, Cryst. Growth Des. 9 (2009) 1474–1480;
(b) S.W. Cao, Y.J. Zhu, J. Phys. Chem. C 112 (2008) 6253–6257.
[13] J. Yu, X. Yu, Environ. Sci. Technol. 42 (2008) 4902–4907.
[14] S. Kment, H. Kmentova, P. Kluson, J. Krysa, Z. Hubicka, V. Cirkva, I. Gregora, O. Solcova, L. Jastrabik, J. Colloid Interface Sci. 348 (2010) 198–205.
[15] W. Choi, A. Termin, M.R. Hoffmann, J. Phys. Chem. 98 (1994) 13669–13679.
[16] N. Murakami, T. Chiyoya, T. Tsubota, T. Ohno, Appl. Catal. A: Gen. 348 (2008) 148–152.
[17] (a) M. Zhou, J. Yu, B. Cheng, J. Hazard. Mater. 137 (2006) 1838–1847;
(b) J. Yu, Q. Xiang, M. Zhou, Appl. Catal. B: Environ. 90 (2009) 595–602.
[18] Y. Yang, X.J. Li, J.T. Chen, L.Y. Wang, J. Photochem. Photobiol. A: Chem. 163 (2004) 517–522.
[19] L. Cui, Y. Wang, M. Niu, G. Chen, Y. Cheng, J. Solid State Chem. 182 (2009) 2785–2790.
[20] S. Kim, S.J. Hwang, W. Choi, J. Phys. Chem. B 109 (2005) 24260–24267.
[21] J.A. Navio, M. Macias, M.G. Gomez, M.A. Pradera, Appl. Catal. B: Environ. 82 (2008) 225–232.
[22] B. Tian, C. Li, F. Gu, H. Jiang, Y. Hu, J. Zhang, Chem. Eng. J. 151 (2009) 220–227.
[23] S. Senthilkumar, K. Porkodi, R. Gomathi, A.G. Maheswari, N. Manonmai, Dyes Pigments 69 (2006) 22–30.
[24] M. Zhou, J. Yu, B. Cheng, H. Yu, Mater. Chem. Phys. 93 (2005) 159–163.
[25] J.C.S. Wu, C.H. Chen, J. Photochem. Photobiol. A: Chem. 163 (2004) 509–515.
[26] T. Ohno, Z. Miyamoto, K. Nashijima, H. Kanemitsu, F. Xueyuan, Appl. Catal. A: Gen. 302 (2006) 62–68.
[27] S. Yin, Y. Aita, M. Komatsu, T. Sato, J. Eur. Ceram. Soc. 26 (2006) 2735–2742.
[28] Y. Park, W. Kim, H. Park, T. Tachikawa, T. Majima, W. Choi, Appl. Catal. B: Environ. 91 (2009) 355–361.
[29] Y. Wang, C. Feng, Z. Jin, J. Zhang, J. Yang, S. Zhang, J. Mol. Catal. A: Chem. 260 (2006) 1–3.
[30] (a) G. Liu, Y. Zhao, C. Sun, F. Li, G.Q. Lu, H.M. Cheng, Angew. Chem. Int. Ed. 47 (2008) 4516–4520;
(b) G. Liu, X. Wang, L. Wang, Z. Chen, F. Li, G.Q.M. Lu, H.M. Cheng, J. Colloid Interface Sci. 334 (2009) 171–175;
(c) G. Liu, L. Wang, C. Sun, X. Yan, X. Wang, Z. Chen, S.C. Smith, H.M. Cheng, G.Q. Lu, Chem. Mater. 21 (2009) 1266–1274;
(d) G. Liu, L. Wang, C. Sun, Z. Chen, X. Yan, L. Cheng, H.M. Cheng, G.Q.M. Lu, Chem. Commun. 11 (2009) 1383–1385;
(e) G. Liu, C. Sun, X. Yan, L. Cheng, Z. Chen, X. Wang, L. Wang, S.C. Smith, G.Q.M. Lu, H.M. Cheng, J. Mater. Chem. 19 (2009) 2822–2829.
[31] (a) A. Zaleska, E. Grabowska, J.W. Sobczak, M. Gazda, J. Hupka, Appl. Catal. B: Environ. 89 (2009) 469–475;
(b) P. Gorska, A. Zaleska, J. Hupka, Sep. Purif. Technol. 68 (2009) 90–96;
(c) A. Zaleska, P. Gorska, J.W. Sobczak, J. Hupka, Appl. Catal. B: Environ. 76 (2007) 1–8.
[32] G. Liu, X. Wang, Z. Chen, H.M. Cheng, G.Q.M. Lu, J. Colloid Interface Sci. 329 (2009) 331–338.
[33] M. Zhou, J. Yu, J. Hazard. Mater. 152 (2008) 1229–1236.
[34] J. Yu, M. Zhou, B. Cheng, X. Zhao, J. Mol. Catal. A: Chem. 246 (2006) 176–184.
[35] L. Lin, R.Y. Zheng, J.L. Xie, Y.X. Zhu, Y.C. Xie, Appl. Catal. B: Environ. 76 (2007) 196–202.
[36] T. Wu, G. Liu, J. Zhao, H. Hidaka, N. Serpone, J. Phys. Chem. B 102 (1998) 5845–5851.
[37] M. Stylidi, D.I. Kondarides, X.E. Verykios, Appl. Catal. B: Environ. 47 (2004) 189–201.

[38] D. Chatterjee, S. Dasgupta, J. Photochem. Photobiol. C: Photochem. Rev. 6 (2005) 186–205.
[39] E. Bae, W. Choi, Environ. Sci. Technol. 37 (2003) 147–152.
[40] F. Chen, Z. Deng, X. Li, J. Zhang, J. Zhao, Chem. Phys. Lett. 415 (2005) 85–88.
[41] L. Wu, J.C. Yu, X. Fu, J. Mol. Catal. A: Chem. 244 (2006) 25–32.
[42] D. Jing, L. Guo, Catal. Commun. 8 (2007) 795–799.
[43] V. Iliev, D. Tomova, R. Todorovska, D. Oliver, L. Petrov, D. Todorovsky, M.U. Bujnova, Appl. Catal. A: Gen. 313 (2006) 115–121.
[44] Z. Wu, Z. Sheng, H. Wang, Y. Liu, Chemosphere 77 (2009) 264–268.
[45] K. Nagaveni, M.S. Hegde, G. Madras, J. Phys. Chem. B 108 (2004) 20204–20212.
[46] J.M. Herrmann, J. Disdier, P. Pichat, Chem. Phys. Lett. 108 (1984) 618–622.
[47] K. Wilke, H.D. Breuer, J. Photochem. Photobiol. A: Chem. 121 (1999) 49–53.
[48] Z. Luo, Q.H. Gao, J. Photochem. Photobiol. A: Chem. 63 (1992) 367–375.
[49] M. Gratzel, R.F. Howe, J. Phys. Chem. 94 (1990) 2566–2572.
[50] W. Mu, J.M. Herrmann, P. Pichat, Catal. Lett. 3 (1989) 73–84.
[51] K.E. Karakitsou, X.E. Verykios, J. Phys. Chem. 97 (1993) 1184–1189.
[52] A.W. Xu, Y. Gao, H.Q. Liu, J. Catal. 207 (2002) 151–157.
[53] L.G. Devi, S.G. Kumar, B.N. Murthy, K. Nagaraju, Catal. Commun. 10 (2009) 794–798.
[54] C. Graf, R.O. Wiedemann, G. Kreisel, J. Photochem. Photobiol. A: Chem. 188 (2007) 226–234.
[55] L.G. Devi, G.M. Krishnaiah, J. Photochem. Photobiol. A: Chem. 121 (1999) 141–145.
[56] L.G. Devi, B.N. Murthy, Catal. Lett. 125 (2008) 320–330.
[57] (a) L.G. Devi, B.N. Murthy, S.G. Kumar, Mater. Sci. Eng. B 166 (2010) 1–6;
(b) L.G. Devi, B.N. Murthy, S.G. Kumar, J. Mol. Catal. A: Chem. 308 (2009) 174–181;
(c) L.G. Devi, N. Kottam, S.G. Kumar, K.E. Rajashekhar, Cent. Eur. J. Chem. 8 (2009) 142–148.
[58] R.A. Spurr, H. Myers, Anal. Chem. 29 (1957) 760–762.
[59] K. Okada, N. Yamamoto, Y. Kameshima, A. Yasumori, K.J.D. MacKenzie, J. Am. Ceram. Soc. 84 (2001) 1591–1596.
[60] H.E. Chao, Y.U. Yun, H.U. Xingfang, A. Larbot, J. Eur. Ceram. Soc. 23 (2003) 1457–1464.
[61] (a) L.G. Devi, K. Nagaraju, S.G. Kumar, K.S.A. Raju, Catal. Lett. 131 (2009) 612–617;
(b) R. Arroyo, G. Cordoba, J. Padilla, V.H. Lara, Mater. Lett. 54 (2002) 397–402;
(c) J.P. Xu, S.B. Shi, L. Li, J.F. Wang, L.Y. Lv, F.M. Zhang, Y.W. Du, J. Phys. Chem. Solids 70 (2009) 511–515;
(d) L.G. Devi, K. Nagaraju, B.N. Murthy, S.G. Kumar, J. Mol. Catal. A: Chem. 328 (2010) 44–52.
[62] A. Burns, G. Hayes, W. Li, J. Hirvonen, J.D. Demaree, S.I. Shah, Mater. Sci. Eng. B 111 (2004) 150–155.
[63] (a) J. Lukac, M. Klementova, P. Bezdicka, S. Bakardijieva, J. Subrt, L. Szatmary, Z. Bastl, J. Jirkovsky, Appl. Catal. B: Environ. 74 (2007) 83–91;
(b) L.C. Chen, C.M. Huang, F.R. Tsai, J. Mol. Catal. A: Chem. 265 (2007) 133–140.
[64] (a) S.G. Hur, T.W. Kim, S.J. Hwang, H. Park, W. Choi, S.J. Kim, J.H. Choy, J. Phys. Chem. B 109 (2005) 15001–15007;
(b) W. Li, Y. Wang, H. Lin, S.I. Shah, C.P. Huang, D.J. Doren, S.A. Rykov, J.G. Chen, M.A. Barteau, Appl. Phys. Lett. 83 (2003) 4143–4145.
[65] Y.V. Pleskov, Sov. Electrochem. 17 (1981) 1–25.
[66] L. Palmisano, V. Augugliaro, A. Sclafani, M. Schiavello, J. Phys. Chem. 92 (1988) 6710–6713.
[67] A. Wold, J. Papp, S. Soled, K. Dwight, Chem. Mater. 6 (1994) 496–500.
[68] Z. Ding, G.Q. Lu, P.F. Greenfield, J. Phys. Chem. B 104 (2000) 4815–4820.
[69] J.C. Yu, J. Lin, R.W.M. Kwok, J. Phys. Chem. B 102 (1998) 5094–5098.
[70] B. Ohtani, Y. Ogawa, S.I. Nishimoto, J. Phys. Chem. B 101 (1997) 3746–3752.
[71] (a) J. Lin, J.C. Yu, D. Lo, S.K. Lam, J. Catal. 183 (1999) 368–372;
(b) J. Yu, S. Liu, M. Zhou, J. Phys. Chem. C 112 (2008) 2050–2057.
[72] J. Li, C.L. Fisher, J.L. Chen, D. Bashford, L. Noodleman, Inorg. Chem. 35 (1996) 4694–4702.
[73] P. Kurzweil, Sensors 9 (2009) 4955–4985.
[74] A.J. Kelly, N. Oyama, J. Phys. Chem. 95 (1991) 9579–9584.
[75] J.B. Miller, S.J. Decanio, J.B. Michel, C. Dybowski, J. Phys. Chem. 89 (1985) 2592–2596.
[76] J. Panpranot, K. Kontapakdee, P. Praserthdam, J. Phys. Chem. B 110 (2006) 8019–8024.
[77] T.V.D. Meulen, A. Mattson, L. Osterlund, J. Catal. 251 (2007) 131–144.
[78] R.R. Basca, J. Kiwi, Appl. Catal. B: Environ. 16 (1998) 19–29.
[79] J. Wang, G. Zhao, Z. Zhang, X. Zhang, G. Zhang, T. Ma, Y. Jiang, P. Zhang, Y. Li, Dyes Pigments 75 (2007) 335–343.
[80] S. Lei, W. Duan, J. Environ. Sci. 20 (2008) 1263–1267.
[81] T. Ohno, K. Sarukawa, K. Tokieda, M. Matsumura, J. Catal. 203 (2001) 82–86.
[82] T. Ohno, K. Tokieda, S. Higashida, M. Matsumura, Appl. Catal. A: Gen. 244 (2003) 383–391.
[83] T. Lopez, R. Gomez, E. Sanchez, F. Tzompantzi, L. Vera, J. Sol-gel Sci. Technol. 22 (2001) 99–107.
[84] Q. Zhang, L. Gao, J. Guo, Appl. Catal. B: Environ. 26 (2000) 207–215.
[85] K.Y. Jung, S.B. Park, H.D. Jang, Catal. Commun. 5 (2004) 491–497.
[86] Y. Bessekhouad, D. Robert, J.V. Weber, J. Photochem. Photobiol A: Chem. 157 (2003) 47–53.
[87] Q. Xiao, Z. Si, Z. Yu, G. Qiu, Mater. Sci. Eng. B 137 (2007) 189–194.
[88] Q. Xiao, Z. Si, J. Zhang, C. Xiao, X. Tan, J. Hazard. Mater. 150 (2008) 62–67.
[89] Q. Xiao, Z. Si, Z. Yu, G. Qiu, J. Alloys Comp. 450 (2008) 426–431.
[90] L. Zhao, M. Han, J. Lian, Thin Solid Films 516 (2008) 3394–3398.
[91] B. Sun, P.G. Smirniotis, Catal. Today 88 (2003) 49–59.
[92] M. Yan, F. Chen, J. Zhang, M. Anpo, J. Phys. Chem. B 109 (2005) 8673–8678.
[93] J.C. Yu, J. Yu, W. Ho, Z. Jiang, L. Zhang, Chem. Mater. 14 (2002) 3808–3816.
[94] J.C. Yu, L. Zhang, J. Yu, Chem. Mater. 14 (2002) 4647–4653.
[95] J.C. Yu, J. Yu, W. Ho, L. Zhang, Chem. Commun. (2001) 1942–1943.
[96] Z. Ambrus, K. Moryorosi, A. Szalai, T. Alapi, K. Demeter, A. Dombi, P. Sipos, Appl. Catal. A: Gen. 340 (2008) 153–161.
[97] G. Li, L. Chen, M.E. Graham, K.A. Gray, J. Mol. Catal. A: Chem. 275 (2007) 30–35.
[98] D.C. Hurum, A.G. Agrios, S.E. Crist, K.A. Gray, T. Rajh, M.C. Thurnauer, J. Electron Spectrosc. Relat. Phenom. 150 (2006) 155–163.
[99] Y. Li, H. Li, T. Li, G. Li, R. Cao, Microporous Mesoporous Mater. 117 (2009) 444–449.
[100] G. Li, S. Ciston, Z.V. Saponjic, L. Chen, N.M. Dimitrijevic, T. Rajh, K.A. Gray, J. Catal. 253 (2008) 105–110.
[101] H. Xu, L. Zhang, J. Phys. Chem. C 113 (2009) 1785–1790.
[102] G. Liu, Z. Chen, C. Dong, Y. Zhao, F. Li, G.Q. Lu, H.M. Cheng, J. Phys. Chem. B 110 (2006) 20823–20828.
[103] G. Tian, H. Fu, L. Jing, C. Tian, J. Hazard. Mater. 161 (2009) 1122–1130.
[104] L. Chen, M.E. Graham, G. Li, K.A. Gray, Thin Solid Films 515 (2006) 1176–1181.
[105] A. Zachariah, K.V. Baiju, S. Shukla, K.S. Deepa, J. James, K.G.K. Warrier, J. Phys. Chem. C 112 (2008) 11345–11356.
[106] C. Wu, Y. Yue, X. Deng, W. Hua, Z. Gao, Catal. Today 93–95 (2004) 863–869.
[107] Y.V. Kolenko, B.R. Churagulov, M. Kunst, L. Mazerolles, C.C. Justin, Appl. Catal. B: Environ. 54 (2004) 51–58.
[108] S. Bakardjieva, J. Subrt, V. Stengl, M.J. Dianez, M.J. Sayagues, Appl. Catal. B: Environ. 58 (2005) 193–202.
[109] L. Chen, J. Zhu, Y.M. Liu, Y. Cao, H.X. Li, H.Y. He, W.L. Dai, K.N. Fan, J. Mol. Catal. A: Chem. 255 (2006) 260–268.
[110] C.K. Chan, J.F. Porter, Y.G. Li, W. Guo, C.M. Chan, J. Am. Ceram. Soc. 82 (1999) 566–572.
[111] B. Jongsomjit, T. Wongsalee, P. Praserthdam, Catal. Commun. 6 (2005) 705–710.
[112] Y. Yu, J.C. Yu, J.G. Yu, Y.C. Kwok, Y.K. Che, J.C. Zhao, L. Ding, W.K. Ge, P.K. Wong, Appl. Catal. A: Gen. 289 (2005) 186–196.
[113] L. Chen, B. Yao, Y. Cao, K. Fan, J. Phys. Chem. C 111 (2007) 11849–11853.
[114] (a) S. Watson, D. Beydoun, J. Scott, R. Amal, J. Nanoparticle Res. 6 (2004) 193–207;
(b) B. Zhao, F. Chen, Q. Huang, J. Zhang, Chem. Commun. (2009) 5115–5117;
(c) J. Yu, M. Zhou, B. Cheng, H. Yu, X. Zhao, J. Mol. Catal. A: Chem. 227 (2005) 75–80;
(d) J. Yu, J. Xiong, B. Cheng, S. Liu, Appl. Catal. B: Environ. 60 (2005) 211–221;
(e) G. Liu, X. Yan, Z. Chen, X. Wang, L. Wang, G.Q.M. Lu, H.M. Cheng, J. Mater. Chem. 19 (2009) 6590–6596.
[115] G. Li, K.A. Gray, Chem. Phys. 339 (2007) 173–187.
[116] N. Serpone, D. Lawless, R. Khariutdinov, E. Pelizzetti, J. Phys. Chem. 99 (1995) 16655–16661.
[117] R. Scotti, I.R. Bellobono, C. Canevali, C. Cannas, M. Catti, M.D. Arienzo, A. Musinum, S. Polizzi, M. Sommariva, A. Testino, F. Morazzoni, Chem. Mater. 20 (2008) 4051–4061.
[118] R.I. Bickley, T.G. Carreno, J.S. Lees, L. Palmisano, R.J.D. Tilley, J. Solid State Chem. 92 (1991) 178–190.
[119] L.G. Devi, N. Kottam, S.G. Kumar, J. Phys. Chem. C 113 (2009) 15593–15601.
[120] D.C. Hurum, A.G. Agrios, K.A. Gray, T. Rajh, M.C. Thurnauer, J. Phys. Chem. B 107 (2003) 4545–4549.
[121] S. Leytner, J.T. Hupp, Chem. Phys. Lett. 330 (2000) 231–236.
[122] X. Hong, Z. Wang, W. Cai, F. Lu, J. Zhang, Y. Yang, N. Ma, Y. Liu, Chem. Mater. 17 (2005) 1548–1552.
[123] P. Bouras, E. Stathatos, P. Lianos, Appl. Catal. B: Environ. 73 (2007) 51–59.
[124] G. Li, N.M. Dimitrijevic, L. Chen, J.M. Nichols, T. Rajh, K.A. Gray, J. Am. Chem. Soc. 130 (2008) 5402–5403.
[125] Z. Zhang, C.C. Wang, R. Zakaria, J.Y. Ying, J. Phys. Chem. B 102 (1998) 10871–10878.
[126] D.Q. Fei, T. Hudaya, A.A. Adesina, Catal. Commun. 6 (2005) 253–258.
[127] R.K. Wahi, W.W. Yu, Y. Liu, M.L. Mejia, J.C. Falkner, W. Nolte, V.L. Colvin, J. Mol. Catal. A: Chem. 242 (2005) 48–56.
[128] Y. Zheng, C. Chen, Y. Zhan, X. Lin, Q. Zheng, K. Wei, J. Zhu, Y. Zhu, Inorg. Chem. 46 (2007) 6675–6682.
[129] J.W. Shi, J.T. Zheng, Y. Hu, Y.C. Zhao, Mater. Chem. Phys. 106 (2007) 247–249.